Geophys. J. Int. (1997) **129**, 252–268

Material versus isobaric internal boundaries in the Earth and their influence on postglacial rebound

Paul Johnston,[1] Kurt Lambeck[1] and Detlef Wolf[2]

[1] *Research School of Earth Sciences, Australian National University, Canberra,* ACT 0200, *Australia. E-mail: paul@rses.anu.edu.au*

[2] *GeoForschungsZentrum Potsdam, Division 1: Kinematics and Dynamics of the Earth, Telegrafenberg* A17, D-14473 *Potsdam, Germany*

Accepted 1996 December 9. Received 1996 November 12; in original form 1994 December 7

SUMMARY

Most previous earth models used to calculate viscoelastic relaxation after the removal of the Late Pleistocene ice loads implicitly assume that there is no exchange of mass across the mantle density discontinuities on periods of tens of thousands of years (the material boundary formulation). In the present study, simple incompressible models are used to determine the Earth's behaviour in the case where the density discontinuity remains at a constant pressure rather than deforming with the material (the isobaric boundary formulation). The calculation of the movement of the boundary is more rigorous than in earlier studies and uses the local incremental pressure calculated at the depth of the boundary and allows for the vertical deformation caused by the change in volume as material changes phase. It is shown that the buoyancy modes associated with the density discontinuities decrease in strength and increase in relaxation time analogous to what results when the density contrast is reduced. Also, two viscoelastic modes arise from an isobaric boundary, which is also predicted when there is a contrast in rigidity or viscosity across a material boundary. The difference in predicted radial deformation between the isobaric boundary model and the material boundary model is largest for long-wavelength loads for which the material incremental pressure at depth is largest. If the isobaric boundary model is appropriate for the treatment of the mineral phase changes in the mantle on glacial rebound timescales, then previous inferences of the deep-mantle to shallow-mantle viscosity ratio based on large-scale deformation (spherical harmonic degree <10) of the Earth and including data from the early part of the glacio-isostatic uplift are too small.

Key words: glacial isostasy, phase transitions, mantle viscosity.

1 INTRODUCTION

The glacial rebound problem associated with the deglaciation of the Late Pleistocene ice sheets has the property that the Earth exhibits both elastic and fluid behaviour on the timescale of interest. Since the Earth takes some time to respond to changes in the glacial and meltwater load at the surface of the Earth, a viscoelastic rheology is commonly used to model the transition from elastic to fluid behaviour. The correspondence principle (Biot 1965; Peltier 1974) states that the Laplace transform of a linear viscoelastic constitutive law is formally identical to the elastic constitutive law, and a viscoelastic problem may be solved by taking the Laplace transform of the complete set of field equations and boundary conditions, solving the equivalent elastic problem, and finally taking the inverse Laplace transform to determine the time dependence of the solution. The correspondence principle may be used to obtain the correct solution of a viscoelastic problem, provided that the corresponding elastic problem is correctly formulated. It has already been shown that the correspondence principle can be validly applied for an initially hydrostatically pre-stressed Earth with density stratification due to self-compression (Wolf 1991b), contrary to earlier claims (Fjeldskaar & Cathles 1984).

The nature of the density discontinuities at 420 km and 670 km depth within the mantle has been widely discussed in the literature (for a recent review, see Jackson & Rigden 1997). It has been argued in the past that the seismic discontinuities are too sharp to be explained solely in terms of phase changes; however, high-pressure experiments on upper mantle and analogue minerals over the last four decades show that a change in chemical composition is not required in order to explain the seismic data (Ringwood 1975; Ito, Takahashi & Matsui 1984; Bina & Wood 1987). If one adopts the position that the mantle is largely chemically homogeneous, then there should be significant mass exchange between the upper and lower mantle, which would indicate that convection velocities

are significant at each boundary. Although it is expected that there is significant mass exchange across the boundaries on convection timescales, if the convection velocity is small or the region over which the phase change occurs is narrow, the latent heat released by the phase change may not be advected or conducted away from the boundary fast enough to allow the phase change (and hence mass exchange) to proceed on glacial rebound timescales (O'Connell & Wasserburg 1967; O'Connell 1976; Mareschal & Gangi 1977; Christensen 1985). In this paper, two alternative models of boundary behaviour are to be tested in relation to the glacial rebound problem. These two end members are for the case where there is no mass exchange across the phase boundary (a material boundary) and the case where the boundary remains at the same pressure (an isobaric boundary). It is assumed that the heat released or absorbed by the phase change is advected away or towards the boundary sufficiently quickly in the second model, so that temperature does not influence the position of the boundary.

There are two important reasons for comparing the two models. The first is to test whether observations relating to glacial rebound can determine the nature of the density discontinuities within the mantle. The second is to determine if previous inferences of viscosity (most of which are based on models which assume a material boundary) are seriously in error, and to place an upper bound on the magnitude of the possible error associated with the assumption of a material boundary. Furthermore, the question of whether the density gradients in the upper mantle that are in excess of that due to self-compression (e.g. Bullen 1975) are caused by changes in mineral composition or changes in chemical composition can be addressed in the same way as the isobaric boundary problem. A region with an excess density gradient may be thought of as a number of small density discontinuities which will behave as material boundaries if the excess density gradient is due to a compositional gradient, or as isobaric boundaries if there is a region of mixed mineral phase with varying proportions of each phase. Therefore, solving the problem of a single isobaric boundary correctly will help in understanding the problem with continuous density variation.

There have been some attempts to consider the effect of a phase boundary (Cathles 1975; Yuen *et al.* 1986) and the related problem of 'adiabatic' density variation (Fjeldskaar & Cathles 1984) for the deformation associated with deglaciation. Cathles (1975) noted that as material changes phase, it changes density and produces radial displacement additional to what would occur if there were a material boundary rather than a phase boundary. However, Cathles (1975) and Fjeldskaar & Cathles (1984) approximated the change in pressure at the internal density discontinuity using the change in pressure at the surface, which is only a reasonable approximation when the wavelength of the load is large compared with the depth of the phase change. Yuen *et al.* (1986) maintained that the buoyancy mode associated with the jump in density is unimportant if the boundary is a phase boundary, but neglected the change in radial displacement due to the change of material to a phase of different density. This paper shows that it is possible to include the changes in pressure and density in a model based on the correspondence principle in a rigorous and systematic manner. The thermodynamic factors that affect the short-term response of the phase boundary will be examined via a response factor, which is an indicator of the degree to which the boundary behaves like an isobar (Christensen 1985). The longer-term conduction of latent heat away from the boundary is not considered, because this process occurs on timescales of the order of a million years and is therefore too slow to be of significance in the glacial rebound problem (O'Connell 1976; Peltier 1985b). The behaviour of phase boundaries for the convection problem has also been studied recently (Dehant & Wahr 1991).

The paper has the following structure. After the derivation of the boundary conditions appropriate to an earth model with phase changes, the effect on the magnitudes and relaxation times of radial deformation is investigated. Radial deformation is the largest contributor to the postglacial uplift of formerly glaciated regions, so it is the quantity of greatest interest geophysically. Also, because the phase change is capable of inducing additional radial deformation (Cathles 1975), it is this quantity that we expect to be most strongly affected by the presence of a phase change. The initial calculations are made with the simplest spherical models in order to determine effects only from the type of density discontinuity and to avoid interference from other effects. Assuming Maxwell viscoelasticity, incompressibility, constant density, shear modulus and viscosity within each layer, analytical solutions can be used to determine the modes of viscoelastic relaxation (Wu & Peltier 1982; Wolf 1994). With these simple solutions, the effect of the nature of an internal density jump can be clearly seen. In Section 2, a brief description is given of the mathematical theory necessary to determine the deformation, including modifications to the existing theory (Wu 1978; Peltier 1985a) to allow a phase boundary within the Earth. In Section 3, the radial displacements are calculated for one-, two- and five-layer models to demonstrate the role of an isobaric boundary. The calculated behaviour of the relaxation modes is used to determine the types of observational data that are likely to be sensitive to the nature of the internal density jumps at 420 and 670 km. In Section 4, comparisons are made between predicted sea-level change, geoid deformation, free-air gravity anomaly and present horizontal velocity due to a simple ice-sheet load in the space–time domain for an earth model with either material or isobaric boundaries in the upper mantle.

2 MATHEMATICAL FORMULATION

2.1 Boundary conditions across a phase boundary

In this section, the boundary conditions to be applied at an internal boundary between homogeneous layers of different densities are derived, where the position of the boundary does not necessarily coincide with a particular material boundary. In other words, matter may cross the boundary and change density. This can occur at the boundary between two phases of material of the same chemical composition, in which case the equilibrium position of the boundary is determined by pressure and temperature. There are essentially two possibilities for the motion of the material and boundary. When displacement of the material is upwards, the boundary movement will be either upwards but by a smaller distance than the displacement, or downwards. The converse is true when the material displacement is downwards. The two end members are the situations where the material initially on the boundary remains on the boundary (i.e. displacement equals boundary movement) and the case where the boundary remains at its initial pressure (isobaric boundary). These two cases are shown in Fig. 1. For

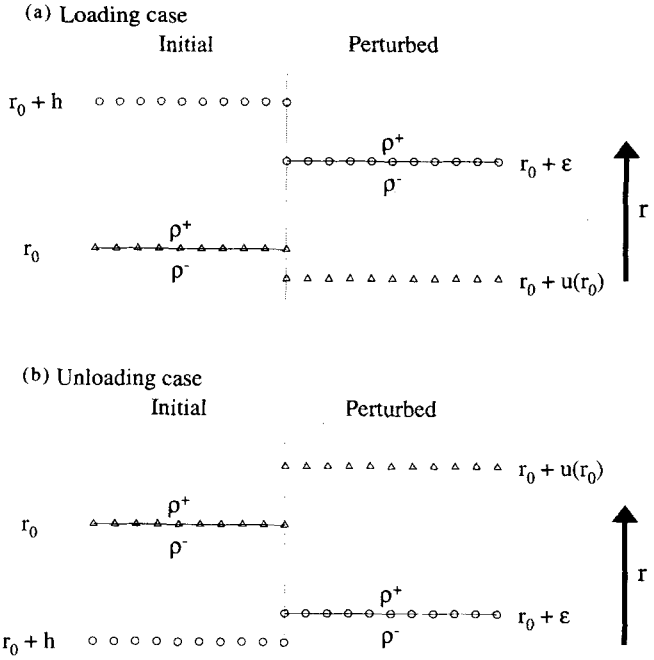

Figure 1. The initial and perturbed state of a phase boundary (a) in the loading case; (b) in the unloading case. The triangles are particles that were initially on the phase boundary, and the circles are particles that are on the boundary in the perturbed state. The solid line indicates the phase boundary, which separates material of density ρ^+ and ρ^-. The figure also shows the definitions of r_0, h, and ε.

each case, the situation is shown for the initial and perturbed conditions. The solid line indicates the position of the phase boundary, while the markers indicate the motion of particles. The positions of two types of particles are marked, namely those that are initially at the boundary and those whose perturbed positions are on the perturbed boundary. These two sets of particles have initial positions r_0 and $r_0 + h$ and final positions $r_0 + u(r_0)$ and $r_0 + \varepsilon$ respectively, where u is the radial displacement. The relationship between h and ε is

$$\varepsilon = h + u(r_0 + h). \tag{1}$$

The case in Fig. 1 with negative (downward) radial displacement is defined as the *loading* case, because when a load is applied at the surface, displacement is negative, while the case with positive radial displacement is termed the *unloading* case.

We wish to find the changes in radial displacement, potential gradient and radial stress which take place across the phase-change region. This may be achieved by integrating the incremental forms of the continuity, gravitational and inertia equations across the region of interest. A slight modification of the usual first-order perturbation theory is necessary in the region of a phase change. In Fig. 1, it is clear that the rate of change of radial displacement $u_{1,1} = \partial u/\partial r$ is much larger than elsewhere in either region. Therefore, it will be treated as first order and all other components $u_{i,j} = \partial u_i/\partial X_j$ will be considered to be second order within the phase-change region.

For perturbations of first order, the continuity equation can be written as (Wolf 1991b, eq. 90)

$$(1 + \nabla\cdot\mathbf{u})(\rho^{(0)} + \rho^{(\delta)}) = \rho^{(0)}, \tag{2}$$

where $\mathbf{u}$ is the displacement, ρ is the density and the superscripts $^{(0)}$, $^{(\delta)}$ and $^{(\Delta)}$ (used below) represent the intial value, the material increment and local increment of a quantity (Wolf 1991b). Keeping only first-order terms, eq. (2) can be rearranged to give

$$u_{1,1} = -\frac{\rho^{(\delta)}}{\rho^{(0)}}. \tag{3}$$

The initial density for both loading and unloading cases is given by

$$\rho^{(0)}(r) = \begin{cases} \rho^-, & r < r_0 \\ \rho^+, & r > r_0 \end{cases}, \tag{4}$$

and the density after perturbation is

$$\rho(r) = \begin{cases} \rho^-, & r < r_0 + h \\ \rho^+, & r > r_0 + h \end{cases}. \tag{5}$$

With these relations, the material increment in density ($\rho^{(\delta)} = \rho - \rho^{(0)}$) is different for the loading and unloading cases. For the loading case (where $h > 0$),

$$\rho^{(\delta)}(r) = \begin{cases} \rho^- - \rho^+, & r_0 < r < r_0 + h \\ 0, & \text{otherwise} \end{cases}, \tag{6}$$

and for the unloading case,

$$\rho^{(\delta)}(r) = \begin{cases} \rho^+ - \rho^-, & r_0 + h < r < r_0 \\ 0, & \text{otherwise} \end{cases}. \tag{7}$$

Then, the radial derivative of the radial component of displacement follows from eq. (3). For the loading case,

$$u_{1,1}(r) = \begin{cases} \dfrac{\rho^+ - \rho^-}{\rho^+}, & r_0 < r < r_0 + h \\ 0, & \text{otherwise} \end{cases}, \tag{8}$$

and for the unloading case,

$$u_{1,1}(r) = \begin{cases} \dfrac{\rho^- - \rho^+}{\rho^-}, & r_0 + h < r < r_0 \\ 0, & \text{otherwise} \end{cases}. \tag{9}$$

To derive the boundary conditions, we invoke the divergence theorem, and integrate over a small pillbox which straddles the boundary (e.g. Cathles 1975). The usual statement of the divergence theorem assumes a vector field in Eulerian coordinates. The correct statement of the divergence theorem for Lagrangian coordinates assuming $u_{i,j}$ is of second order except for $u_{1,1}$, which is of first order, is derived in Appendix A, and is applied for the pillbox integration of a first-order vector field. The boundary conditions for a general first-order vector field are given for the loading and unloading cases in eqs (A8) and (A9) respectively.

To obtain the boundary conditions for radial displacement at a phase boundary in the loading case, eq. (8) is substituted into eq. (A8) to obtain

$$u^+ - u^- = (\varepsilon - u^-)\frac{\rho^+ - \rho^-}{\rho^+}. \tag{10}$$

Note that, in the loading case, u^+ and u^- have been defined as $u(r_0 + h)$ and $u(r_0)$ respectively. In the unloading case, eq. (9)

is substituted into eq. (A9) leading to

$$u^+ - u^- = (u^+ - \varepsilon)\frac{\rho^- - \rho^+}{\rho^-},$$

$$\frac{\rho^+}{\rho^-}u^+ = u^- + \frac{\rho^+ - \rho^-}{\rho^-}\varepsilon,$$

$$u^+ - u^- = (\varepsilon - u^-)\frac{\rho^+ - \rho^-}{\rho^+}. \tag{11}$$

In the unloading case, u^+ and u^- have been defined as $u(r_0)$ and $u(r_0 + h)$ respectively. Therefore, the boundary condition for radial deformation is the same for both the loading and unloading cases.

The incremental equation for the gravitational potential correct to first order when deformations are of first or higher order is

$$\nabla\cdot(\nabla\phi^{(\Delta)} - 4\pi G\rho^{(0)}\mathbf{u}) = 0 \tag{12}$$

(Longman 1962; Wolf 1991b), where ϕ is the gravitational potential and G is the gravitational constant. Defining

$$q = (\nabla\phi^{(\Delta)} - 4\pi G\rho^{(0)}\mathbf{u})_r = \frac{\partial\phi^{(\Delta)}}{\partial r} - 4\pi G\rho^{(0)}u, \tag{13}$$

the boundary condition for q is the same for the loading and unloading cases. After consideration of eqs (12) and (13) in eq. (A8) or (A9), the boundary condition is

$$q^+ - q^- = 0, \tag{14}$$

with the superscripts $^+$ and $^-$ of q taking on the same meanings as for the radial displacement.

Finally, to obtain the boundary conditions for the radial stress, the divergence theorem should be applied to the inertia equation. The incremental inertia equation to first order is

$$t^{(\delta)}_{ij,j} + (p^{(0)}_{,j}u_j)_{,i} - \phi^{(0)}_{,i}(\rho^{(0)}u_j)_{,j} + \rho^{(0)}\phi^{(\Delta)}_{,i} = 0 \tag{15}$$

(e.g. Wolf 1991b). Since $g^{(0)}_i = \phi^{(0)}_{,i}$ is implied in eq. (15), the magnitude of initial gravity is $g^{(0)} = -\partial\phi^{(0)}/\partial r$. Making the substitution $f_j = t_{1j} + \rho^{(0)}g^{(0)}u_j$ in eq. (A8), the boundary condition for the loading case is

$$\begin{aligned} t^{(\delta)+}_{rr} - t^{(\delta)-}_{rr} + g^{(0)}(\rho^+u^+ - \rho^-u^-) &= \int_{r_0+u(r_0)}^{r_0+\varepsilon}\frac{\partial}{\partial r}(\rho^{(0)}g^{(0)}u_r) - \rho^{(0)}\frac{\partial\phi^{(\Delta)}}{\partial r}\,dr \\ &= g^{(0)}(\rho^+u^+ - \rho^-u^-) - (\varepsilon - u^-)\rho^+\frac{\partial\phi^{(\Delta)}}{\partial r}(r_0). \end{aligned} \tag{16}$$

Since there is no sharp gradient in $\phi^{(\Delta)}$ across the phase boundary, its derivative is of the same order as the non-radial derivatives of displacement, i.e. second order. Therefore, we obtain the boundary condition

$$t^{(\delta)+}_{rr} - t^{(\delta)-}_{rr} = 0 \tag{17}$$

correct to second order. The same boundary condition is obtained for the unloading case.

Physically, the boundary conditions (14) and (17) state that the phase boundary has only a second-order effect on the radial stress and gravity. The physical meaning of the apparent jump in radial displacement (10) is that there is a change in volume as material crosses the phase boundary.

The only difference between the phase boundary conditions (10, 14, 17) and the usual material boundary conditions is in the apparent discontinuity in radial displacement. This result contradicts the assumption of Yuen *et al.* (1986), who assume continuity of radial displacement and discontinuity of material incremental stress.

The material boundary conditions are actually contained within the more general boundary conditions developed here by setting the displacement u^- and phase boundary movement ε to be equal. In this case, the displacement is continuous as it should be. It is also salient to note that a discontinuity in radial displacement does not mean that there is cavitation or overlap of mass at the boundary. It just represents the change in volume undergone by the material which changes phase.

It remains now to specify how far the phase boundary moves. The simplest model is to assume that the boundary remains at constant pressure, which neglects the temperature dependence of the phase boundary. This model also assumes that material changes instantaneously in response to a change in pressure. The first assumption has a minor effect on the distance by which the phase boundary moves. The second one has a larger effect, since, realistically, latent heat produced by the phase change may significantly change the temperature at the boundary causing the pressure at which the phase change occurs to be modified (O'Connell & Wasserburg 1967; O'Connell 1976; Mareschal & Gangi 1977; Christensen 1985). A modification of the model will be discussed later in Sections 2.2 and 3.3 to allow for temperature dependence of the phase boundary.

If the boundary is assumed to remain at constant pressure, then the following equation holds:

$$p^{(0)}(r_0) = p(r_0 + h) = p^{(0)}(r_0 + \varepsilon) + p^{(\Delta)}(r_0 + \varepsilon). \tag{18}$$

The local increment in pressure $p^{(\Delta)}$ is discontinuous across a density discontinuity. The change across the boundary is given by

$$\begin{aligned} (p^{(\Delta)})^+ - (p^{(\Delta)})^- &= (p^{(\delta)})^+ - (p^{(\delta)})^- + g(\rho^+u^+ - \rho^-u^-) \\ &= (\rho^+ - \rho^-)g\varepsilon. \end{aligned} \tag{19}$$

Also, since after perturbation, $r_0 + \varepsilon$ and $r_0 + h$ are on the same side of the boundary,

$$p^{(\Delta)}(r_0 + \varepsilon) = p^{(\Delta)}(r_0 + h) \tag{20}$$

to first order. In the loading case,

$$\begin{aligned} p^{(0)}(r_0) &= p^{(0)}(r_0 + \varepsilon) + p^{(\Delta)}(r_0 + \varepsilon) \\ &= p^{(0)}(r_0) - p^+g\varepsilon + (p^{(\Delta)})^+ \\ &= p^{(0)}(r_0) - \rho^+g\varepsilon + (p^{(\Delta)})^- + (\rho^+ - \rho^-)g\varepsilon, \end{aligned}$$

$$\varepsilon = \frac{(p^{(\Delta)})^-}{\rho^-g}, \tag{21}$$

while, in the unloading case,

$$\begin{aligned} p^{(0)}(r_0) &= p^{(0)}(r_0 + \varepsilon) + p^{(\Delta)}(r_0 + \varepsilon) \\ &= p^{(0)}(r_0) - \rho^-g\varepsilon + (p^{(\Delta)})^-, \end{aligned}$$

$$\varepsilon = \frac{(p^{(\Delta)})^-}{\rho^-g}. \tag{22}$$

So the distance by which the phase boundary moves is the same for each case. The distance by which the phase boundary moves relative to the material is

$$\varepsilon - u^- = \frac{(p^{(\Delta)})^- - \rho^-gu^-}{\rho^-g} = \frac{(p^{(\delta)})^-}{\rho^-g}, \tag{23}$$

which is the same expression as that derived by Dehant & Wahr (1991), ignoring temperature effects. This means that the distance by which the phase boundary moves relative to the material is proportional to the change in pressure experienced by a particle at the depth of the phase change. The material incremental pressure $p^{(\delta)}$ at depth is smaller than the pressure applied at the surface by a load and the amount of attenuation depends strongly on the wavelength of the load. The method employed by Cathles (1975) approximates the material incremental pressure by the surface load, which is only a good approximation when the depth of the phase change is much less than the wavelength of the load.

2.2 Elastic problem for incompressible layered models

The problem of calculating the deformation for a spherically symmetric elastic earth model is a classical one and has been discussed at length in the literature. In this paper, the spectral approach is employed, whereby forces resulting from changes in the surface load are decomposed into spherical harmonic components; the response function for each component is calculated and then combined with the components of the load to determine the deformation. If the earth model consists of uniform incompressible layers, analytic solutions for each layer can be used to calculate the deformation. For a viscoelastic earth model, the elastic solutions are used to determine the viscoelastic solution via the correspondence principle. So we begin by calculating the deformation for a sphere consisting of elastic layers with an optional fluid innermost layer (core).

As usual, the six variables describing the spherical harmonic coefficient of the degree-n component of the spheroidal mode of deformation—radial (u_n) and tangential (v_n) displacement, material increments of radial (t_{rn}) and tangential ($t_{\theta n}$) stress, local increment in gravitational potential (ϕ_n) and the modified local increment of gravity (q_n)—form a vector that satisfies the system of differential equations in Runge–Kutta form:

$$\frac{d\mathbf{y}^n}{dr} = A^n \mathbf{y}^n, \tag{24}$$

where r is the radial distance, the matrix A^n is given in Longman (1963) or Wu & Peltier (1982), for example, (but the incompressible limit must be taken), and

$$\mathbf{y}^n = (u_n, v_n, t_{rn}, t_{\theta n}, \phi_n, q_n)^{\mathrm{T}}. \tag{25}$$

The six linearly independent solutions to the system of differential equations for homogeneous, incompressible regions are given by Sabadini, Yuen & Boschi (1982), Spada *et al.* (1990) and Wu (1990). Here, the solution presented by Wu (1990) is used except that the third component of the first solution should have a plus sign before the factor 2μ. The first three solutions contain factors of r^n, while the last three contain factors of r^{-n}. In a layered earth, the solution for the loading problem can be obtained by applying the regularity conditions at the centre of the earth and boundary conditions at the surface and at the interfaces between adjacent layers. The method is described in detail in the three papers just mentioned.

Since the six linearly independent solutions span the solution space, the general solution within a layer may be written as a linear combination of the six solutions. For each layer i extending from r_{i-1} to r_i, the solution vectors $\mathbf{y}^n_{ij}(r), j = 1, 2, \ldots, 6$ are defined in terms of the properties of that layer, namely its density ρ_i and rigidity μ_i. If M^n_i is the matrix with the six solution vectors $\mathbf{y}^n_{ij}, j = 1, 2, \ldots, 6$ as columns, then the general solution in the ith layer is

$$\mathbf{y}^n(r) = M^n_i(r)\mathbf{c}^i, \qquad r_{i-1} \le r \le r_i, \tag{26}$$

where $\mathbf{c}^i$ is the coefficient vector for layer i.

At the boundary between two layers, boundary conditions specify how the deformation changes from one layer to the next. At any boundary across which there is no exchange of mass, all six components of $\mathbf{y}^n$ are continuous. At an isobaric boundary, the boundary conditions derived in the previous section must be imposed.

The equilibrium position of the phase boundary depends on a number of factors including the local change in pressure, the Clapeyron slope of the phase change, and the temperature gradient. The rate at which the phase boundary moves to its equilibrium position depends on several other factors such as the latent heat of the phase change, whether the phase change consists of two phases (univariant) or several intermediate phases (divariant) and the rate at which heat is carried away from the boundary. Without convection, conduction of heat away from the interface has a characteristic time of the order of one million years and therefore has little effect during a single glacial cycle (O'Connell 1976; Peltier 1985b). With reasonable mantle convection velocities (vertical velocities across the boundary of 1 cm yr^{-1}), most of the phase change proceeds very quickly compared with glacial rebound timescales (Christensen 1985) for a univariant phase change because the convection creates a region at least several kilometres thick of mixed phase within which the latent heat is released or absorbed, rather than a sharp interface (Turcotte & Schubert 1971). Christensen (1985) showed that, when the conduction of heat is neglected (which is reasonable for timescales up to 100 kyr), the phase boundary moves to a position somewhere between its original position relative to the material (i.e. no material changing phase) and the position with the same pressure as the original phase boundary. The new position is determined by thermodynamic properties of the material and the latent heat release of the phase change. The movement to the new position should occur instantaneously. The displacement of the boundary relative to the material is

$$\varepsilon - u^- = \xi \frac{(p^{(\delta)})^-}{\rho^- g}, \tag{27}$$

where ξ is the response factor which lies between 0 and 1 and depends on the type of phase change (divariant or univariant), Clapeyron slope, specific heat, width of phase change region, density jump and temperature at the boundary (Christensen 1985). A boundary with a response factor of 0 is a material boundary, while a response factor of 1 means that the boundary remains at the same pressure. In the first set of calculations to follow, a response factor of 1 will be used to determine the maximum possible effect of a phase boundary, and in later calculations, measured values of the thermodynamic parameters will be used to determine the response factor. The degree n spherical harmonic component of eq. (27) is

$$\begin{aligned}\varepsilon_n - u_n^- &= \xi \frac{(p_n^{(\delta)})^-}{\rho^- g} = \xi \frac{2\mu^- u_n'^- - t_{rn}}{\rho^- g} \\ &= \xi \frac{-4\mu u_n^-/r + 2n(n+1)\mu v_n/r - t_{rn}}{\rho^- g},\end{aligned} \tag{28}$$

where u_n' is the radial derivative of u_n. The second equality on

the first line follows from the elastic constitutive equation and the last step uses the components of the matrix A^n in eq. (24).

At an internal boundary, continuity conditions imply a relationship between the coefficients of the solution vectors for each layer, which also depend on the nature of the boundary. If ξ_i is the response factor for the boundary at r_i, a general boundary condition can be written, which applies to both material and isobaric boundaries. The continuity condition is

$$M^{i+1}(r_i)\mathbf{c}^{i+1} = (I + \xi_i \boldsymbol{\alpha}_i \boldsymbol{\beta}_i^{\mathrm{T}}) M^i(r_i)\mathbf{c}^i, \tag{29}$$

where I is the identity matrix and the two vectors $\boldsymbol{\alpha}_i$ and $\boldsymbol{\beta}_i$ are, respectively, the coefficients required to determine the jump in properties and the value of the boundary displacement relative to the material. Their components are

$$\boldsymbol{\alpha}_i^{\mathrm{T}} = (\Delta\rho_i/\rho_{i+1}, 0, 0, 0, 0, 0), \tag{30}$$

$$\boldsymbol{\beta}_i^{\mathrm{T}} = (-4\mu_i/r_i, 2n(n+1)\mu_i/r_i, -1, 0, 0, 0)/(\rho_i g(r_i)), \tag{31}$$

where $\Delta\rho_i = \rho_{i+1} - \rho_i$ is the density jump at r_i. The application of boundary conditions at the surface and core–mantle boundary and the regularity conditions are given in Wu (1990).

2.3 Correspondence principle

If the rheology of the mantle is linear viscoelastic instead of elastic and the perturbations are quasi-static, the full set of field equations, constitutive equations and boundary conditions may be Laplace-transformed to produce equations that are identical in form to the elastic equations with the rigidity replaced by an equivalent function in the Laplace-transformed constitutive equation (Biot 1965; Peltier 1974).

The treatment of the boundary conditions in Section 2.1 is entirely independent of the rheology of the material since the constitutive equation was not used. Therefore, the boundary conditions are valid for both a solid and fluid and the correspondence principle may be used to solve the viscoelastic problem with phase boundaries contrary to the arguments of Cathles (1975) and Fjeldskaar & Cathles (1984). They argue that different incremental inertia equations are valid for a fluid and solid. However this cannot be true, because it would imply that Newton's second law is different for different materials. Wolf (1991b) demonstrated that the apparent difference in the incremental equations is a result of using the material incremental stress for a solid material and the local incremental stress for a fluid material. When the same incremental stress is used for both fluid and solid, the same inertia equation results. Therefore, we routinely apply the correspondence principle to calculate the solution for a viscoelastic earth.

For a Heaviside load history $H(t)$, the degree-n component of the solution for a viscoelastic earth is

$$\mathbf{y}^{nH}(r, t) = H(t)\left(\mathbf{y}^{nE}(r) + \sum_{j=1}^{K} \frac{\mathbf{R}_j^n(r)}{-s_j^n}[1 - \exp(s_j^n t)]\right), \tag{32}$$

where $\mathbf{y}^{nE}$ is the initial elastic response to the load, calculated from the elastic equations, K is the number of relaxation modes, $-1/s_j^n$ is the relaxation time and $\mathbf{R}_j^n/(-s_j^n)$ is the strength of the jth mode.

3 RELAXATION MODES FOR UNIFORM AND LAYERED EARTH MODELS

A rigorous study of the effects of various factors such as density, rigidity or viscosity contrast, the presence of a core or lithosphere and lithospheric thickness for layered, incompressible Maxwell viscoelastic earth models with material internal boundaries has been made before (Wu & Peltier 1982; Wolf 1984, 1985; Amelung & Wolf 1994). A couple of simple models (which are not assumed to be realistic) will be used for comparison with previous results and to give standard models with which to compare the models with isobaric boundaries.

In the following figures of relaxation modes, the strengths of the modes are normalized by the density and thickness of the load, so that if a spherical harmonic load of density ρ_L and thickness $LY_n(\theta, \lambda)$ were applied at the surface, the radial deformation would be

$$u(\theta, \lambda, t) = \rho_L L Y_n(\theta, \lambda) H(t)\left(\bar{u}^{nE} + \sum_{j=1}^{K} \frac{\bar{u}_j^n}{-s_j^n}[1 - \exp(s_j^n t)]\right), \tag{33}$$

where θ and λ are the colatitude and longitude, and the values plotted in the figures are the normalized elastic radial displacement $\bar{u}^{nE}$ and the normalized strengths of viscoelastic radial displacement $\bar{u}_j^n/(-s_j^n)$. The geoid deformation is also proportional to the load and is given by

$$G(\theta, \lambda, t) = \frac{\rho_L L}{g} Y_n(\theta, \lambda) H(t)\left(\bar{\phi}^{nE} + \sum_{j=1}^{K} \frac{\bar{\phi}_j^n}{-s_j^n}[1 - \exp(s_j^n t)]\right). \tag{34}$$

$\bar{\phi}^{nE}$ and $\bar{\phi}_j^n/(-s_j^n)$ are plotted in the figures. The displacement in the θ (southerly) direction for the same load is

$$v(\theta, \lambda, t) = \rho_L L \frac{\partial Y_n}{\partial \theta}(\theta, \lambda) H(t)\left(\bar{v}^{nE} + \sum_{j=1}^{K} \frac{\bar{v}_j^n}{-s_j^n}[1 - \exp(s_j^n t)]\right). \tag{35}$$

For the special case where the load is centred at the pole, $Y_n(\theta, \lambda) = P_n(\cos\theta)$ and the derivative is $-\sin\theta P_n'(\cos\theta)$ where $P_n'(x) = \partial P_n(x)/\partial x$. At the pole, $P_n'(1) = n(n+1)/2$. So, in the figures $n(n+1)\bar{v}^{nE}/2$ and $n(n+1)\bar{v}_j^n/-2s_j^n$ are plotted, which gives the approximate magnitude of the maximum horizontal displacement as a function of spherical harmonic degree.

3.1 Uniform model

The simplest model to be considered is a uniform incompressible Maxwell viscoelastic sphere. Such a model, when subjected to a Heaviside load of spherical harmonic degree, deforms elastically with the initial deformation determined by the density, rigidity and spherical harmonic degree, and then relaxes towards a state of hydrostatic equilibrium with a single relaxation time, which is determined by the density, rigidity, viscosity and spherical harmonic degree. The final deformation depends only on the density and spherical harmonic degree. The results for the radial and horizontal displacement and geoid deformation at the surface are plotted in Fig. 2. The relaxation time for the single mode (labelled M0) increases with spherical harmonic degree almost linearly on the log–log scale as observed by others (Haskell 1935; McConnell 1965), where the departure from linearity for low degrees is due to the inclusion of initial stress (Wolf 1991a). The role of this mode is to produce hydrostatic equilibrium at the surface of the Earth and its strength is governed by the density contrast at the Earth's surface. The nomenclature for modes is the same as that used in the literature (Peltier 1976; Wu & Peltier 1982).

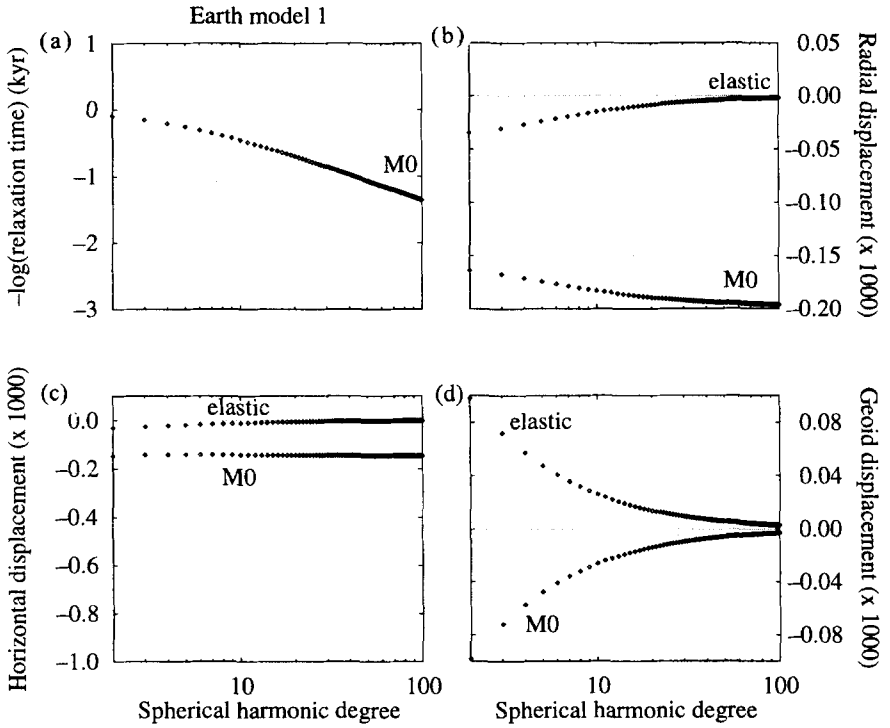

Figure 2. The relaxation modes of a uniform incompressible Maxwell viscoelastic earth model (model 1, Table 1) as a function of spherical harmonic degree. (a) Relaxation time for the M0 mode; (b), (c) and (d) the normalized magnitude of elastic and M0 viscoelastic mode of radial, horizontal and geoid deformation at the surface. See text for normalization.

The final hydrostatic state for the Heaviside loading history of a uniform or multilayered earth model is the sum of the elastic deformation and the magnitudes of all viscoelastic modes [the limit as $t \rightarrow \infty$ in eq. (32)]. Since there is no elastic lithosphere in this uniform model that would partially support the load by elastic forces, the radial deformation at the surface, once equilibrium is attained, is equal to $-1/\rho_s$, where ρ_s is the density of the uppermost (surface) layer. Therefore, in Fig. 2(b), the sum of the elastic deformation and the M0 mode of deformation is equal to $-1/\rho_s = -0.1980$. As the wavelength decreases, the initial elastic response becomes smaller, and the viscoelastic mode is responsible for almost all of the radial and horizontal displacement. Because, on a fluid earth, the load displaces precisely its own weight, the final displacement of the geoid is zero. It is initially positive because of the attraction to the load which is only partially compensated by the elastic deformation.

3.2 Two-layer models

Two very simple models are examined to illustrate the effects of a density discontinuity which is either a material or isobaric boundary. The results for a model with a density jump of approximately 10 per cent across a material boundary (model 2) are compared with the uniform model (model 1) and a model with the same density jump across an isobaric boundary (model 3). A constant shear modulus and viscosity are assumed, so that the relaxation modes are caused only by the density jump at the surface and at 670 km depth. The density for the uniform model is chosen to be slightly less than the average value for the Earth, so that the density of the surface layer is the same for both the uniform and two-layer models, and, therefore, the hydrostatic limit is the same for all three models.

For model 2 (Fig. 3), the density contrast at 670 km depth produces a second relaxation mode, labelled M1, with relaxation times approximately 100 times longer than those for the M0 model (Wu & Peltier 1982). If, in this model, there were also a contrast in rigidity or viscosity at the internal boundary, there would be two further relaxation modes with small magnitude and short relaxation time. The boundary at 670 km depth has negligible effect on the relaxation time of the M0 mode as well as on the magnitude of elastic deformation. Since the sum of the modes plus elastic deformation must equal the hydrostatic limit for the radial deformation, the M1 mode carries some of the deformation which was carried by the M0 mode in the uniform model, particularly at low spherical harmonic degree. Its strength decreases as spherical harmonic degree increases, because the deformation for higher degrees is restricted to the shallower parts of the earth, so that the effect of the boundary becomes less important for higher degrees. With each new density jump in the earth, a new mode is introduced, which ensures that in the final state each material boundary is horizontal (Peltier 1976; Wu & Peltier 1982; Wolf 1985). The M1 mode, when added to the others, ensures that the 670 km discontinuity is horizontal after final relaxation. It contributes upward displacement at this boundary to counteract the depression caused by the elastic and M0 modes. The density contrast in model 2 forces the flow in the mantle to be shallower than for the uniform model, which increases the horizontal displacement at the surface. This can be seen from the very strong contribution by the M1 mode to the total horizontal displacement for long-wavelength loads. For the geoid displacement at the surface, the M1 mode is more than

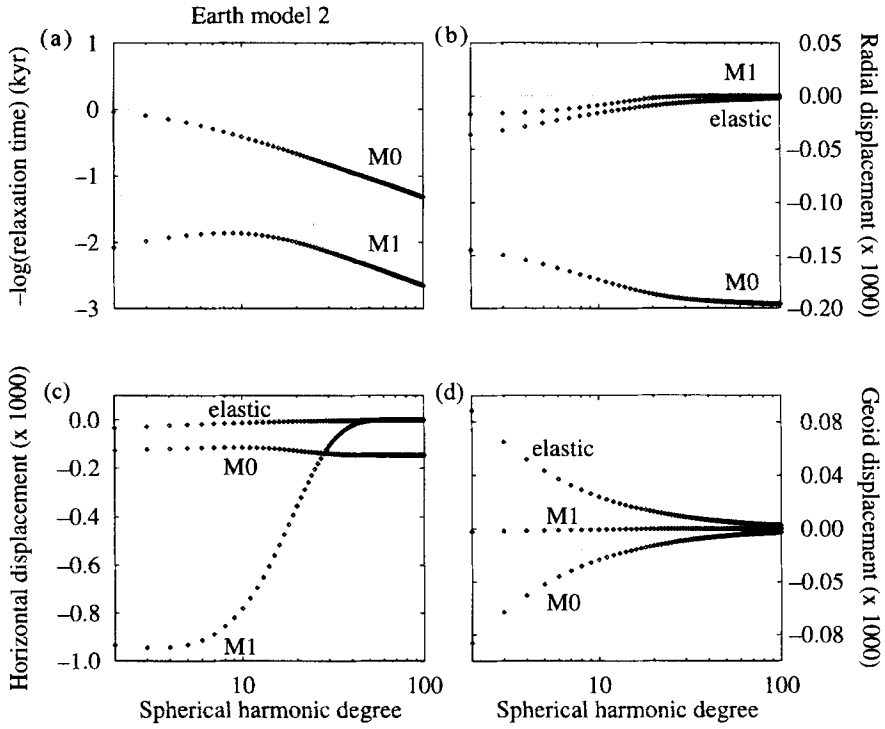

Figure 3. The relaxation modes of a two-layer earth model with a material boundary at 670 km depth (model 2, Table 1). (a) Relaxation time for the M0 and M1 modes; (b), (c) and (d) the normalized magnitude of elastic deformation and M0 and M1 viscoelastic modes of radial, horizontal and geoid deformation at the surface.

an order of magnitude weaker than the M0 mode. This is to be expected since the deficit of mass due to the negative radial displacement at the surface is larger than the mass deficit at 670 km and the effect due to the mass deficit at depth is diminished by its distance from the surface.

In model 3, where the density jump is associated with an isobaric boundary (Fig. 4), the condition that the density jump be a flat surface in the hydrostatic limit is relaxed, because the buoyancy force caused by the deformed boundary is balanced by the weight of material which changes phase. In the hydrostatic limit, the local increment in pressure $p^{(\Delta)}$ is zero, because there can be no horizontal pressure gradients in a system in equilibrium. Therefore the material increment in density is non-zero, so from eq. (23), the final position of the boundary is not equal to the displacement and some material permanently changes phase (in Fig. 6 below, the material boundary at 670 km returns to its initial position, but the isobaric boundary remains deformed). The initial elastic radial displacement at low spherical harmonic degrees is larger than in the material boundary case because material changes from the less dense upper mantle phase to the more dense lower mantle phase. At higher spherical harmonic degrees, there is virtually no difference between models 2 and 3 because the internal boundary is undeformed by short-wavelength loads at the surface. The relaxation time and amplitude of the M0 mode are only marginally affected by the nature of the internal density contrast, since the M0 mode is due mostly to the density jump at the earth's surface. When the boundary is completely isobaric ($\xi = 1$), there is no M1 mode, although for values less than 1 there is an M1 mode that has a longer relaxation time than for the material boundary case ($\xi = 0$), and weaker radial and geoid deformation (see Fig. 5). This behaviour is very similar to the dependence of the relaxation time and modal strength on density contrast for a material boundary. For a two-layer earth model with material boundary, the relaxation time increases and the radial and geoid deformation mode strengths decrease with decreasing density contrast (Wolf 1985; Wu & Ni 1996). In model 3, there are also two very weak relaxation modes, with strengths approximately 100 times and 10^8 times weaker than for the M0 mode. The first one is labelled P1 for the phase boundary and has a relaxation time which depends on spherical harmonic degree and is shorter than the relaxation time of the M1 mode in model 2. The second very weak viscoelastic mode V1 has relaxation time equal to the viscoelastic Maxwell time of earth model 3 ($=\eta/\mu$). The horizontal motion associated with the P1 and V1 modes is very weak because the isobaric boundary does not inhibit radial deformation as it does for the material boundary model. This characteristic difference between models 2 and 3 suggests that horizontal motion is the best observation to use to try to constrain the nature of the mantle density discontinuities from postglacial isostatic adjustment. For geoid deformation, the elastic and M0 modes are almost indistinguishable from those of model 2, so the displacement of the geoid is insensitive to the nature of the internal density discontinuity. For values of ξ less than one, there is virtually no difference in the magnitude of horizontal motion, but the relaxation time of the dominant M1 mode is longer. The difference is only strong when ξ is close to 1 (Fig. 5). In other treatments of a phase boundary, it has been assumed that there would be no restoring force at the phase boundary, which can be achieved by neglecting the M1 mode (Yuen *et al.* 1986; Wu 1990). This seems to provide a good approximation

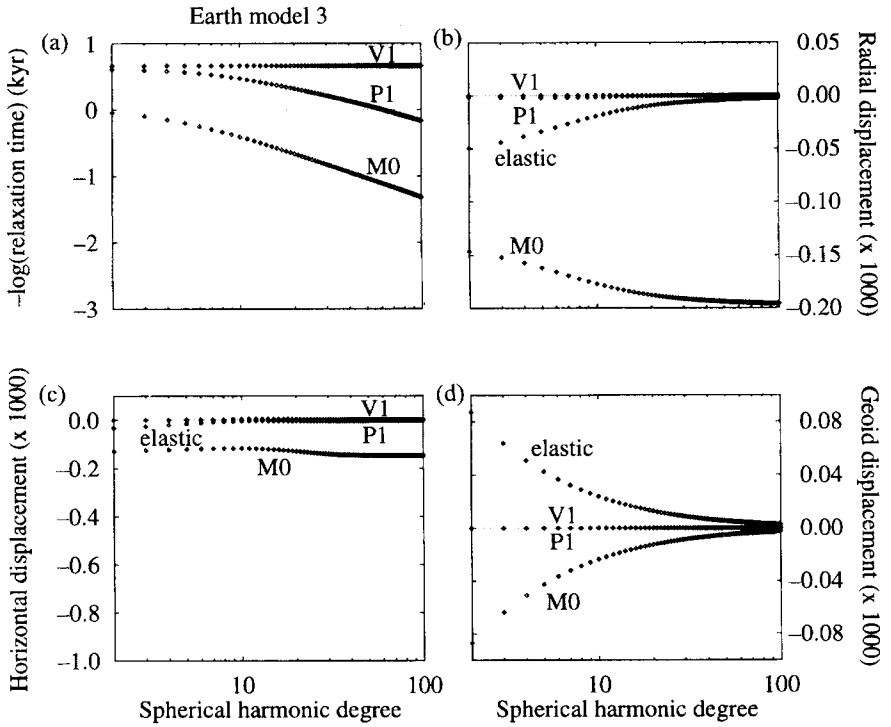

Figure 4. The relaxation modes of a two-layer earth model with an isobaric boundary at 670 km depth (model 3, Table 1). (a) Relaxation time for the M0, P1 and V1 modes; (b), (c) and (d) the normalized magnitude of elastic and M0, P1 and V1 viscoelastic modes of radial, horizontal and geoid deformation at the surface.

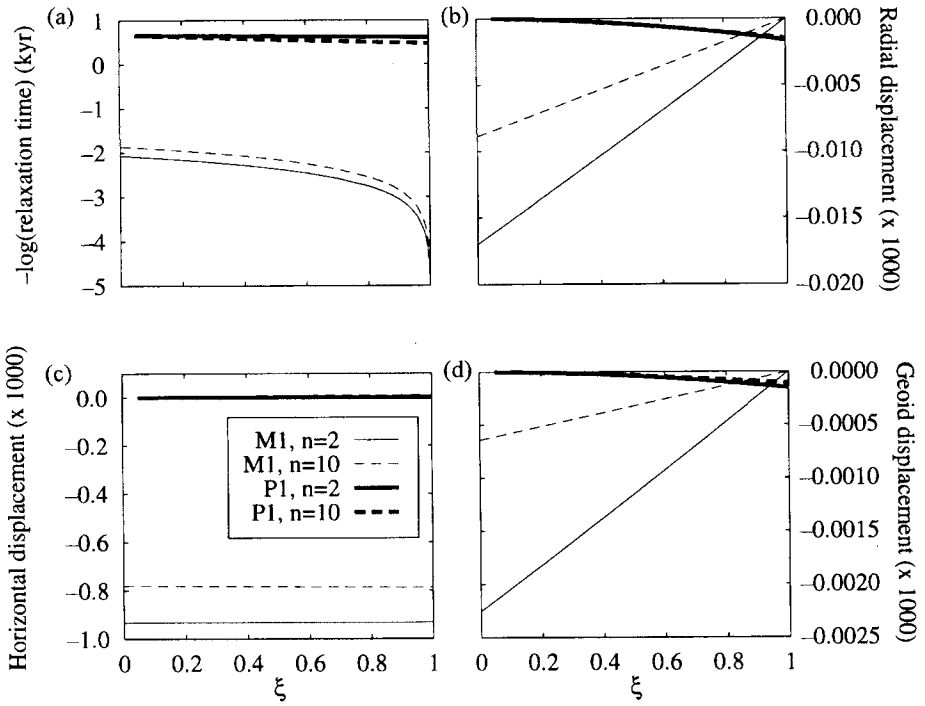

Figure 5. The M1 and P1 relaxation modes for spherical harmonic degrees 2 and 10 of a two-layer earth model with a density discontinuity at 670 km depth varying the response factor ξ. Other parameters are the same as for earth model 2 (Table 1). (a) Relaxation time; (b), (c) and (d) the normalized magnitude of viscoelastic modes of radial, horizontal and geoid deformation at the surface.

of the viscous part of the motion but neglects the enhanced initial displacement.

Fig. 6 shows a comparison of the radial deformation at the 670 km depth discontinuity and at the outer surface for the two-layer earth models 2 and 3. The deformation is in response to a Heaviside load history for three different spherical harmonic degrees. In all cases, there is an initial elastic displacement, which is largest for the surface deformation and lowest

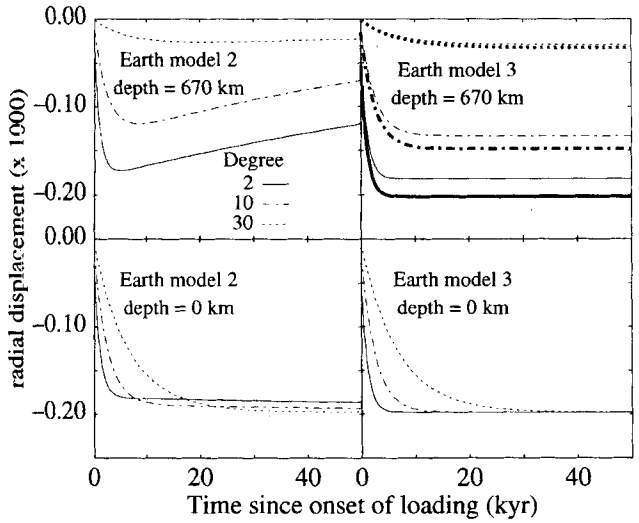

Figure 6. The radial deformation of the uniform and two-layer models as a function of time for Heaviside loads of degree 2, 10 and 30. The two left figures are for model 2 and the two on the right for model 3. The two top figures are the deformation below and above the internal density discontinuity, and the two bottom figures show the surface deformation. In the top right figure, the deformation above the region of mass exchange is shown with thick lines.

spherical harmonic degree. For model 2 (see also Fig. 3), the M0 mode has a relatively short relaxation time of about 1.1 kyr for degree 2 and about 6.6 kyr for degree 30. It reduces in strength with depth, and the attenuation is greater for higher spherical harmonic degree. The M1 mode has a much longer relaxation time of about 100 kyr, which also reduces in strength with increasing spherical harmonic degree. However, at the 670 km discontinuity, it has a larger strength than at the surface and is equal in strength to the elastic plus M0 deformation and opposite in sign, so that, in the final hydrostatic state, there is no deformation of the density discontinuity. Since Fig. 6 only shows the first 50 kyr of deformation, we only see the beginning of the return of the boundary to its undeformed state as was also observed by Wu (1990).

In comparison, the isobaric boundary model 3 does not require that the final state of the density discontinuity at 670 km depth be undeformed, since the exchange of mass between the two layers balances the buoyancy force caused by the deformation of the boundary. Therefore, the M1 mode plays no role in the deformation, and the approach to hydrostatic equilibrium is governed by the relaxation time of the M0 mode, which is a few thousand years for degree 2 and about 30 kyr for degree 30.

3.3 Multilayer earth models

The inclusion of a lithosphere and core produces two additional relaxation modes (L and C), the behaviour of which has been discussed in the literature (Wu & Peltier 1982; Wolf 1985). The presence of a lithosphere also modifies the behaviour of the M0 mode at high spherical harmonic degrees, by reducing its strength and relaxation time. Additional density jumps within the mantle behave in a similar fashion to the density jump described in the two-layer earth model.

Within the framework of a multilayer incompressible laterally homogeneous earth model, the most realistic parameters possible have been chosen to model the earth as the five-layer earth models 4 and 5. One of the important factors controlling the magnitude and relaxation time of a relaxation mode for a material boundary is the change in density across the interface (Wolf 1985). To obtain the approximate behaviour of the real Earth, it is more important to use realistic values for the density jump (including the jump at the surface) than for the actual density. This is because the current model is incompressible, and density only increases with depth via density jumps. Therefore, density jumps in the earth models can be made to match the density jumps in the real Earth, but the density increase due to self-compression cannot be included. This results in a model that is less dense in the deeper layers than in the real Earth. The density model used in earth models 4 and 5 is based on the density profile of PREM (Dziewonski & Anderson 1981), in which the density increase from factors other than self-compression is about 750 kg m^{-3}. In the PREM model, there are jumps of 180 kg m^{-3} and 390 kg m^{-3} at the 420 km and 670 km discontinuities, respectively, and a superadiabatic density gradient in the transition zone and other parts of the upper mantle. In models 4 and 5, the density increase in the mantle occurs only at the boundaries at 420 km and 670 km depth. The total density increase of 750 kg m^{-3} is attained by increases of 250 kg m^{-3} and 500 kg m^{-3} at the 420 km and 670 km depth boundaries, respectively. The two models also include a 120 km thick elastic lithosphere with a jump in density and rigidity at the mantle–lithosphere boundary which is assumed to be associated with a change in chemical composition and includes the effect of the Moho discontinuity. Although the thickness of the lithosphere may be somewhat large compared with several inferences from sea-level change (Wolf 1993; Lambeck *et al.* 1996), its effect has little impact on the low-degree deformation. At the core–mantle boundary, the same density jump (4340 kg m^{-3}) as given in PREM is used, the core is assumed to be inviscid (thus neglecting the solid inner core), and the boundary is assumed to be a material one. Two different models for the viscosity contrast at 670 km depth are used, one with a moderate increase in viscosity (model 4) and one with a strong increase (model 5). The values of the parameters are given in Table 1.

Using models 4 and 5, comparison is made between models where there is mass exchange across the internal boundaries or there is no mass transport for two possible viscosity models. By also comparing the two models with different viscosity contrast, it can be determined whether viscosity contrast or mass exchange across the boundary has a greater influence on the surface deformation. For the models with mass exchange, thermodynamic parameters are used to determine the response factor ξ at the 420 km and 670 km boundaries within the mantle. In the case of a univariant phase transition, the boundary does not behave completely as an isobar ($\xi = 1$), and the response factor is (Christensen 1985)

$$\xi = \max\left(0, 1 - \frac{(\rho^+)^3 g \kappa c_p}{Tw(\rho^- - \rho^+)(dP_c/dT)^2}\right), \tag{36}$$

where κ is thermal diffusivity, c_p specific heat at constant pressure, T the absolute temperature, w the vertical component of the background convection velocity and dP_c/dT is the Clapeyron slope, which gives the rate of change of the pressure of the phase change with respect to temperature. Values of the

Table 1. Properties of layered incompressible earth models used in the calculations.

Model	Radius of boundary (km)	Density (kg/m^3)	Rigidity (Pa)	Viscosity (Pa s)	Response factor of boundary
1	6371	5051	1.45×10^{11}	10^{21}	0
2	5701	5611	1.45×10^{11}	10^{21}	0
	6371	5051	1.45×10^{11}	10^{21}	0
3	5701	5611	1.45×10^{11}	10^{21}	1
	6371	5051	1.45×10^{11}	10^{21}	0
4	3480	8490	0	0	0
	5701	4150	1.50×10^{11}	5×10^{21}	0 or 0.7
	5951	3650	8.70×10^{10}	10^{21}	0 or 0.7
	6251	3400	6.70×10^{10}	10^{21}	0
	6371	2900	4.55×10^{10}	∞	0
5	3480	8490	0	0	0
	5701	4150	1.50×10^{11}	2×10^{22}	0 or 0.7
	5951	3650	8.70×10^{10}	5×10^{20}	0 or 0.7
	6251	3400	6.70×10^{10}	5×10^{20}	0
	6371	2900	4.55×10^{10}	∞	0
6	3486	11100	0	0	0
	5701	4900	2.30×10^{11}	2.0×10^{22}	0
	5931	3800	1.45×10^{11}	1.0×10^{21}	0
	6251	3550	7.10×10^{10}	1.0×10^{21}	0
	6371	2900	4.00×10^{10}	∞	0
7	same viscosity as model 4, but with PREM density, rigidity and compressibility				

parameters used and references to their measurements are given in Table 2. These values give a response factor of approximately 0.7 for both boundaries. Given the uncertainty in the experimental values in Table 2, the response factor is set to 0.7 for both boundaries, when the boundary is assumed to be a phase boundary. Note that the sign of the Clapeyron slope does not directly enter the calculation of the response factor, so the response factor is about the same for both an exothermic or endothermic phase change. It should also be noted that the convection velocity used is probably too large for the region underneath the former Laurentide or Fennoscandian ice sheets, because maximum vertical mantle convection velocities are expected beneath regions which have surface expressions of upwelling (spreading ridges) or sinking (subduction zones). The former ice sheets are not located close to either feature on the Earth's surface. A smaller convection velocity would lead to a smaller response factor ξ and a model which behaves more like the material boundary model. The property which is most closely related to the response factor is the width over which there is mixed phase (Christensen 1985). Seismological observations indicate that the 400 km discontinuity is quite sharp with the boundary layer being resolved to less than 5 to 7 km, while the 670 km discontinuity is approximately 20 to 30 km thick (Petersen *et al.* 1993). If the region of steep seismic velocity gradients is equivalent to the phase change region, then we would expect a response factor close to 1 for the 670 km discontinuity and a much lower value for the 420 km boundary. This suggests that a much larger range of response factors should be tested, but the results below show that the response factor is a much less important parameter than mantle viscosity in determining the radial deformation and sea-level change in response to glacial loads.

Table 2. Thermodynamic properties used in the calculation of the response factors at the 420 km and 670 km discontinuities.

Property	Value	Reference
$dP_c/dT(420)$	3.6×10^6 Pa/K	Ringwood (1991)
$dP_c/dT(670)$	-3×10^6 Pa/K	Akaogo & Ito (1993)
$T(420)$	1700 K	Akaogo & Ito (1993)
$T(670)$	1800 K	Akaogo & Ito (1993)
w	3×10^{-10} m s^{-1}	Christensen (1985)
κ	10^{-6} m^{-3} s^{-1}	Christensen (1985)
c_p	1.25×10^3 J/K/kg	Mao *et al.* (1991)

There are nine relaxation modes for the five-layer models with material boundaries [as was also found by Spada *et al.* (1990)] and also nine modes for the models with mass exchange across the boundary. For material boundaries, each density discontinuity gives rise to a relaxation mode (labelled M) and each discontinuity in rigidity or viscosity causes two relaxation modes—the 'transition' (T) modes in the nomenclature of Wu & Peltier (1982)—except at the core–mantle and lithosphere–mantle boundaries, where the infinite viscosity contrast gives rise to only one mode (respectively, the C and L modes). The numbers 0, 1 and 2 refer to modes due to the boundary at the surface, 670 km depth and 420 km depth respectively. At a phase boundary, the mode due to the density contrast has a longer relaxation time than the corresponding material boundary mode. There is also one P mode and one V mode for each phase boundary. The P modes generally have longer relaxation times than the corresponding T modes. Also, whereas for material boundaries the inverse relaxation times (s_j^n) are always negative and real, when there is more than one phase boundary, the V modes can appear as complex conjugate pairs of zeroes with complex conjugate residues with negative real parts (between degrees 24 and 49 for model 4). The combined response of such a pair of modes is always real, being the product of an exponential and cosine function. The relaxation times for viscosity model 4 with either chemical or phase boundaries are shown in Fig. 7. Where there are complex modes, only the real part is plotted. Although the V modes are very weak, the existence of complex modes is puzzling and presumably is a result of interaction between the two phase boundaries.

4 EFFECT OF PHASE BOUNDARIES ON PREDICTIONS OF OBSERVABLE DATA

From the above examples, we may expect to see differences in the predictions of geophysically observable phenomena for models depending on whether the major density boundaries within the mantle behave like material or isobaric boundaries. These differences are caused by the fact that most of the strength of the viscoelastic radial and geoid deformation for an isobaric boundary model is carried by the surface relaxation mode (M0), instead of partly by internal relaxation modes (M1 and M2) (*cf.* Figs 3 and 4) and that the amplitude of elastic radial deformation is larger for the isobaric model. For the horizontal deformation, most of the viscoelastic deformation for long wavelengths for the material boundary model is carried by the internal modes, for which the relaxation times are much longer and the amplitudes larger than for the M0 mode, which carries all the horizontal deformation for the isobaric boundary model. Therefore, the radial deformation for long-wavelength loads will obviously occur faster for isobaric boundary models than for material boundary models. The lack of an M1 mode of horizontal deformation in the isobaric boundary model reduces horizontal velocity pre-

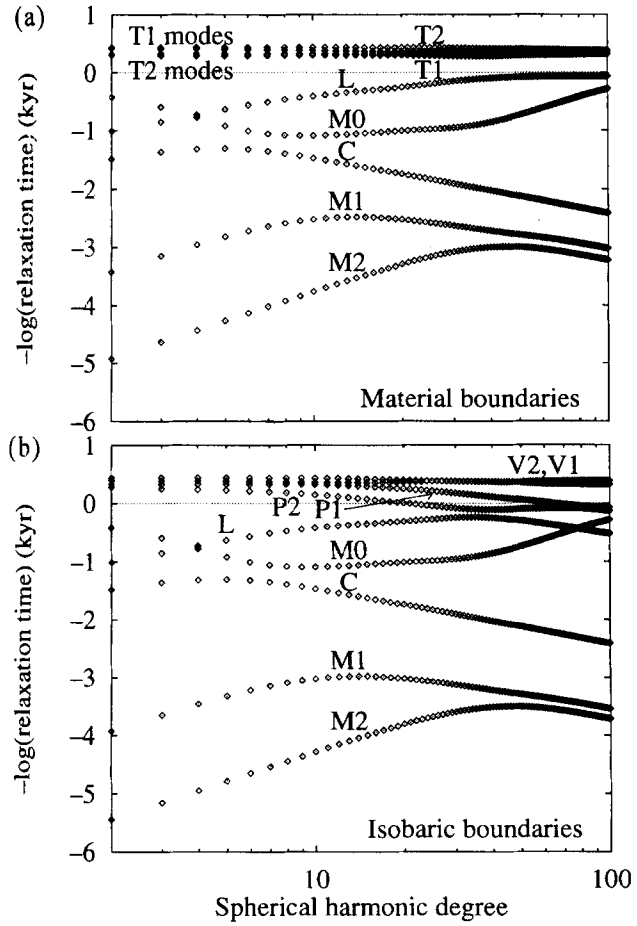

Figure 7. The relaxation modes for the five-layer earth model 4. (a) Material boundaries ($\xi = 0$); (b) partially isobaric boundaries ($\xi = 0.7$). Between degrees 24 and 49, the real part of the complex conjugate pair of zeroes is plotted.

dictions, but only slightly because the relaxation time is so long for the M1 mode. Changing the viscosity profile of the mantle can achieve similar results by modifying the relaxation times of the various modes at different wavelengths. Therefore it is not clear that it will be possible to determine both the mantle viscosity and the nature of internal density contrasts from geophysical observations of postglacial rebound.

The main way of observing Earth deformation resulting from the unloading of the Pleistocene glaciers is via sea-level change, which has a component of radial deformation and geoid change and gives a history of deformation through time. Observations that are sensitive to the response to very long-wavelength loads, such as the Laurentide ice sheet or the meltwater load over the oceans, will exhibit the largest differences in sea-level predictions between the two types of earth model. Below, predictions of sea-level change for a load equal in size to the Laurentide ice sheet for the two different types of internal boundary model are compared to see whether the differences are large enough to require different mantle viscosity profiles to predict the same sea-level curve for the different internal boundary models, or whether there is a possibility of determining to what degree the internal boundaries behave like isobars. Comparisons are also made of predictions for the geoid anomaly and free-air gravity anomaly and horizontal motion.

4.1 Sea-level change

Calculations of sea-level change have been carried out for an axisymmetric ice load which has a maximum radius of 2000 km (18°), an elliptic profile with a maximum thickness of 2800 m and a melting history since the last interglacial equivalent in volume to the North American part of the ICE1 model (Peltier & Andrews, 1976). Prior to the last glacial maximum, eight previous glacial cycles were included, each with build-up of ice taking 90 000 years, deglaciation in 12 000 years and an 8000 year interglacial period. The penultimate deglaciation (128–116 ka BP) was identical to the last one (18–6 ka BP), and earlier glaciations were simplified by melting the entire ice sheet without retreat of the margins. Fig. 8 shows the semi-profile of the ice sheet for the final deglaciation and the volume of the ice sheet (in terms of equivalent sea-level) as a function of time. The method for sea-level calculation uses the classical theory (Farrell & Clark 1976), which has also been described for the particular case of an axisymmetric model (Johnston 1993). Only the component due to the changing ice load (and

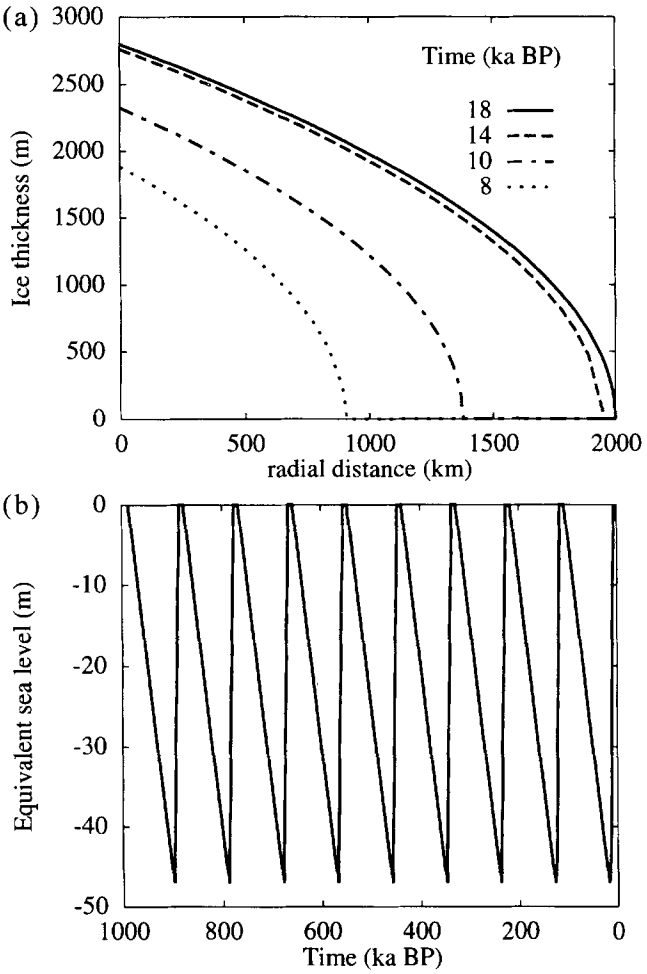

Figure 8. The axisymmetric ice model used for prediction of geophysical observables. (a) Semi-profile of the ice sheet for the last deglaciation; (b) periodic changes in the ice volume in terms of metres of equivalent sea-level change.

not the corresponding change in eustatic sea-level or meltwater load) is plotted for each of the geophysical observables in this and the following sections.

A comparison of sea-level change predictions due to the ice load history is shown in Fig. 9 for the final part of the deglaciation and the two viscosity (4 and 5) and boundary-type models. The model with mass exchange across the boundary ($\xi = 0.7$) differs most from the material boundary model in the glaciated region before the melting is complete because the elastic response to the load is enhanced and the response to the unloading is faster. Also, a larger deformation occurs at the glacial maximum, because the phase boundary model has no long-period relaxation modes to prevent equilibrium from being attained and the deformation is enhanced due to lighter phases transforming to more dense phases within the mantle. After deglaciation is complete (at 6 ka BP), the relative sea-level change is fairly insensitive to the existence of a phase boundary, because the elastic response is no longer important and the internal relaxation modes are of secondary importance compared with the M0 mode. The form of the sea-level change for the isobaric boundary model is not distinctly different from that of the material boundary model, and if a material boundary model fits the sea-level observations, one could also find an isobaric boundary model with higher viscosity which also fits the data and vice versa.

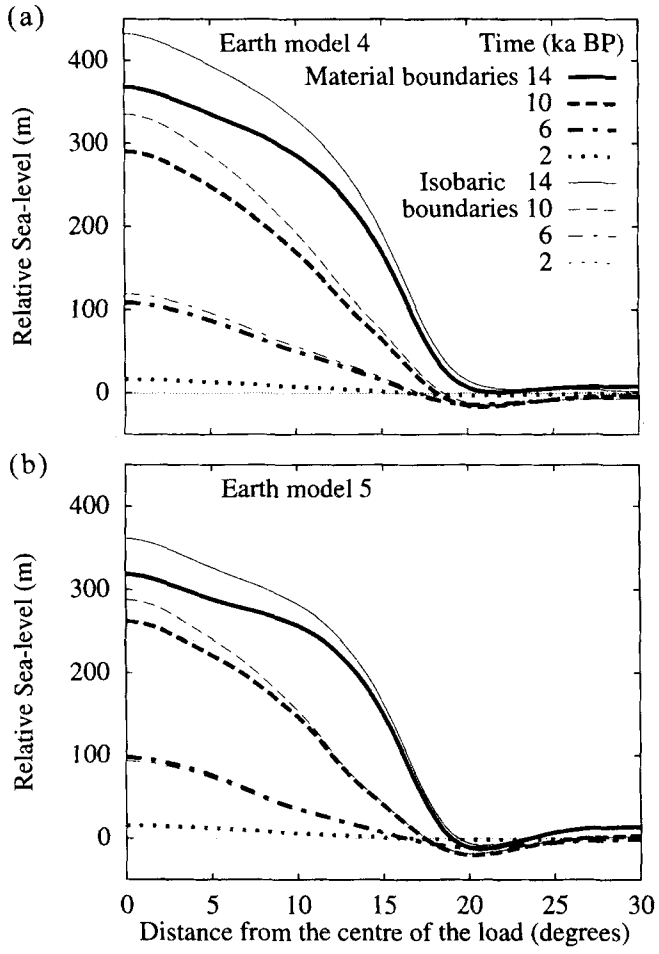

Figure 9. The predicted sea-level change in the near-field of the ice sheet for different rheological models. (a) Earth model 4; (b) earth model 5.

In particular, the sea-level curve at the centre of deglaciation for viscosity model 4 with the material boundary closely resembles that for the isobaric boundary with viscosity model 5. Therefore, it seems unlikely that sea-level data alone would be able to establish conclusively the nature of the mantle density discontinuities, even if the ice melting history were very well constrained.

The presence of an isobaric boundary may explain some of the differences in inferences of mantle viscosity structure from postglacial rebound observations. Rebound predictions for large-radius ice loads, based on the material boundary formulation, tend to give lower viscosity contrasts between the upper and lower mantle (Tushingham & Peltier 1992; Nakada & Lambeck 1991) than do similar predictions for small-radius ice loads (Lambeck 1993a; Lambeck *et al.* 1996) for which the assumption about the nature of the boundary is less important and where the limited resolution for the lower mantle viscosity comes largely from observations during the postglacial stage (Lambeck 1993b). The more usual explanations for the differences in mantle viscosity inferences are that the mantle varies laterally (e.g. Nakada & Lambeck 1991) or that the upper mantle viscosity (above 670 km depth) was held fixed in some studies leading to estimates with small viscosity contrasts (Lambeck *et al.* 1996; Mitrovica 1996). By searching a larger model space it has been possible to find viscosity models which fit a range of rebound observations (e.g. Forte & Mitrovica 1996; Peltier & Jiang 1996), so the difference in mantle viscosity inferences may possibly be an artefact of the inversion procedure.

4.2 Geoid and free-air gravity anomalies

Fig. 10 shows the predicted present geoid anomaly and free-air gravity anomaly due to the deglaciation history (Fig. 8). The free-air gravity anomaly is calculated using the method described by Mitrovica & Peltier (1989). The difference between models 4 and 5 is stronger than the difference between the material and isobaric models. Most of the anomalies are due to the M0 mode, but the difference between the material and isobaric case shows that the relaxation of the M1 mode makes a small contribution to the anomalies in the material boundary case compared with the very small (because $\xi \neq 1$) contribution of the M1 mode for a phase boundary. Although the magnitude of the M1 mode is more than an order of magnitude less than that of the M0 mode (Fig. 3), its relaxation time is much longer, so that, at a time after deglaciation greater than the relaxation time of the M0 mode, it is responsible for more than one-tenth of the geoid anomaly for the material boundary model.

4.3 Horizontal motion

Fig. 11 shows the predicted horizontal motion for viscosity models 4 and 5. As for the geoid and free-air gravity anomalies, the prediction is more strongly influenced by variations of the mantle viscosity parameter in the model over a plausible range of values than by the nature of the internal density discontinuities. As mentioned above, realistic values of the density jump were used rather than the density itself. James & Morgan (1990) used realistic values of the density in an incompressible mantle and obtained predictions of present-day velocities of up to 4.3 mm yr^{-1}, which is much larger than

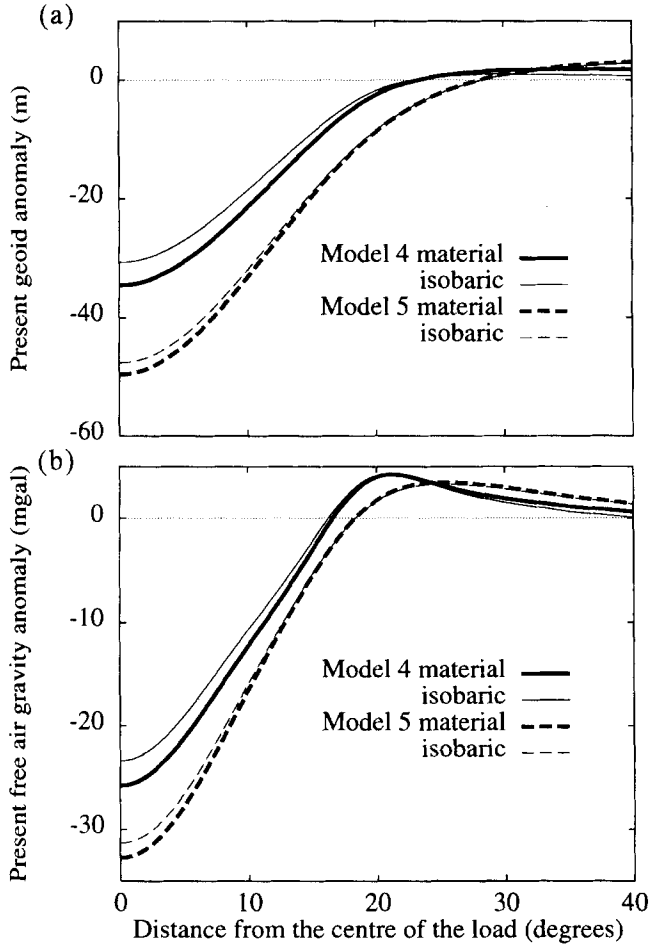

Figure 10. The predicted present geoid anomaly (a) and free-air gravity anomaly (b) for the two different viscosity models (4 and 5) and the material and partially isobaric boundary conditions.

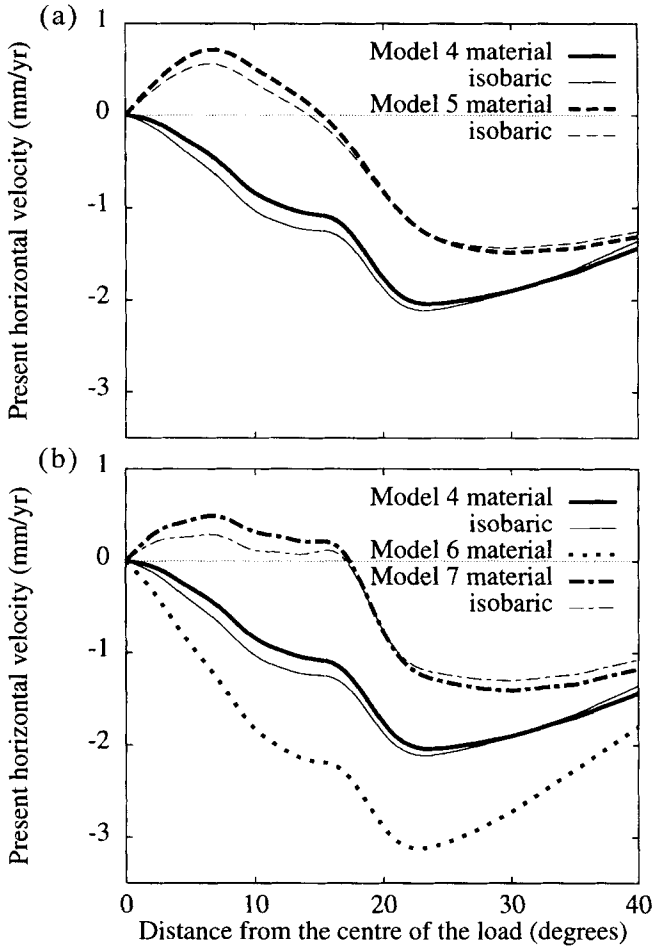

Figure 11. The predicted present-day horizontal velocity in response to the melting of the Laurentide-sized axisymmetric ice sheet. (a) Models with different viscosity profiles; (b) models with different density profiles and compressibility.

the values predicted for model 4 or 5. When using their density and viscoelastic model (earth model 6, Table 1), a maximum horizontal velocity of more than 3 mm yr^{-1} is predicted. Their ice model is 10 per cent thicker than the one employed here, which only partially explains the difference between their predictions and the ones in this paper. Since the viscosity of model 6 lies between that of models 4 and 5, the larger horizontal motion is due to the larger density jumps in model 6.

In a recent study, James & Lambert (1993) predict present outward velocity for much of the area beneath the former Laurentide ice sheet using a compressible earth model. In Fig. 11, model 7 has the same viscosity structure as model 4, but with a compressible lithosphere and mantle. As in James & Lambert, our results confirm that the horizontal velocity can be quite different and even of opposite sign for a compressible model which is identical to an incompressible model in every other respect.

5 CONCLUSIONS

A rigorous calculation of the effects of an isobaric boundary on the viscoelastic relaxation of a layered incompressible earth model has been made which includes the calculation of the increment in pressure at the boundary and the displacement caused by the change in density of material as it passes through the boundary. Contrary to previous claims (Fjeldskaar & Cathles 1984), it is possible to include the effect of phase changes into viscoelastic earth models via the correspondence principle, provided that the boundary conditions at these boundaries are correctly formulated. Models with isobaric boundaries produce larger and faster postglacial uplift than models of the same viscosity structure with material boundaries for long-wavelength loads. A completely isobaric boundary has no buoyancy mode, but a partially isobaric boundary does have a buoyancy mode which has weaker radial and geoid deformation responses and a longer relaxation time than the corresponding buoyancy mode associated with a material boundary. Two very weak viscoelastic modes also arise from an isobaric boundary, one of which is similar to the 'transition' modes, which occur when there is a viscosity or rigidity contrast at a material boundary. The other is extremely weak and would not be detectable in any observation. When there are two isobaric boundaries, there may be a complex conjugate pair of very weak modes for some intermediate spherical harmonic degrees.

If the isobaric boundary model applies for the mantle density discontinuities, previous inferences of mantle viscosity from postglacial uplift would be modified, particularly for larger loads. The behaviour of a material boundary model can be

largely reproduced by an isobaric boundary model with a more viscous deep mantle. However, for all of the geophysical observables examined, mantle viscosity has a stronger effect on the predictions than the nature of the density discontinuity. It must be borne in mind that viscosity inferences based on observations of glacial rebound give effective values for time-scales of 10^3–10^5 years and length-scales of hundreds to thousands of kilometres, and implicitly depend on model assumptions. Models using material boundaries give an effective viscosity profile that is influenced by unmodelled effects such as isobaric boundaries, lateral variation in viscosity (Gasperini & Sabadini 1989), transient (Peltier, Drummond & Tushingham 1986; Yuen *et al.* 1986; Rümpker & Wolf 1996) and non-linear rheology (Wu 1992) and ice model limitations (Lambeck 1993a). If the isobaric boundary model is appropriate for modelling phase changes on glacial rebound time-scales, then deep mantle viscosity inferences determined from the uplift due to melting of large glacial loads such as the Laurentide ice sheet using a material boundary (e.g. Wu & Peltier 1983) underestimate the actual value if data from prior to the end of the deglaciation history is used. This result provides yet another mechanism to explain why no substantial increase in viscosity has been inferred from the North American sea-level record, yet is expected from the correlation of geoid highs with subducted slabs (Hager 1984) and from microphysics (e.g. Sammis *et al.* 1977).

As one goes further back in time, the differences between the two types of boundary models become larger, but the uncertainties in ice load history become larger too. The more recent part of the sea-level record can be used to constrain the viscosity model, while examination of the early part of the sea-level record and other geophysical observations, such as the present horizontal velocity and the geoid anomaly, should provide additional constraints to discriminate between material and isobaric boundaries. Because the effect on different geophysical observables is not the same, there is some hope that phase boundaries could be detected, given excellent constraints on load and uplift history.

ACKNOWLEDGMENTS

Financial support for PJ was provided by the NOP project and Rijkswaterstaat of the Netherlands. Patrick Wu is thanked for a thorough review of the original manuscript and for use of his programs to check the calculations.

REFERENCES

Akaogo, M. & Ito, E., 1993. Heat capacity of $MgSiO_3$ perovskite, *Geophys. Res. Lett.*, **20,** 105–108.

Amelung, F. & Wolf, D., 1994. Viscoelastic perturbations of the earth: significance of the incremental gravitational force in models of glacial isostasy, *Geophys. J. Int.*, **117,** 864–879.

Bina, C.R. & Wood, B.J., 1987. Olivine–Spinel transitions: experimental and thermodynamic constraints and implications for the nature of the 400-km seismic discontinuity, *J. geophys. Res.*, **92,** 4853–4866.

Biot, M.A., 1965. *Mechanics of Incremental Deformations,* John Wiley and Sons, New York, NY.

Bullen, K.E., 1975. *The Earth's Density,* Chapman and Hall, London.

Cathles, L.M., 1975. *The Viscosity of the Earth's Mantle,* Princeton University Press, Princeton, NJ.

Christensen, U.R., 1985. Mantle phase transitions and postglacial rebound, *J. geophys. Res.*, **90,** 11 312–11 318.

Dehant, V. & Wahr, J.M., 1991. The response of a compressible, non-homogenous Earth to internal loading: Theory, *J. Geomag. Geoelectr.*, **43,** 157–178.

Dziewonski, A.M. & Anderson, D.L., 1981. Preliminary reference Earth model, *Phys. Earth planet. Inter.*, **25,** 297–356.

Farrell, W.E. & Clark, J.A., 1976. On postglacial sea level, *Geophys. J. R. astr. Soc.*, **46,** 647–667.

Fjeldskaar, W. & Cathles, L.M., 1984. Measurement requirements for glacial uplift detection of nonadiabatic density gradients in the mantle, *J. geophys. Res.*, **89,** 10 115–10 124.

Forte, A.M. & Mitrovica, J.X., 1996. New inferences of mantle viscosity from joint inversion of long-wavelength mantle convection and post-glacial rebound data, *Geophys. R. Lett.*, **23,** 1147–1150.

Gasperini, P. & Sabadini, R., 1989. Lateral heterogeneities in mantle viscosity and post-glacial rebound, *Geophys. J.*, **98,** 413–428.

Hager, B.H., 1984. Subducted slabs and the geoid: Constraints on mantle rheology and flow, *J. geophys. Res.*, **89,** 6003–6015.

Haskell, N.A., 1935. The motion of a viscous fluid under a surface load, *Physics,* **6,** 265–269.

Ito, E., Takahashi, E. & Matsui, Y., 1984. The mineralogy and chemistry of the lower mantle: an implication of the ultrahigh-pressure phase relations in the system MgO-FeO-SiO_2, *Earth planet. Sci. Lett.*, **67,** 238–248.

Jackson, I. & Rigden, S., 1997. Composition and temperature of the mantle: constraints from experimental studies of Earth materials, in *The Earth's Mantle: Structure, Composition and Evolution—the Ringwood Volume,* ed. Jackson, I., Cambridge University Press, Cambridge, in press.

James, T.S. & Lambert, A., 1993. A comparison of VLBI data with the ICE-3G glacial rebound model, *Geophys. Res. Lett.*, **20,** 871–874.

James, T.S. & Morgan, W.J., 1990. Horizontal motions due to post-glacial rebound, *Geophys. Res. Lett.*, **17,** 957–960.

Johnston, P., 1993. The effect of spatially non-uniform water loads on prediction of sea-level change, *Geophys. J. Int.*, **114,** 615–634.

Lambeck, K., 1993a. Glacial rebound of the British Isles—I. Preliminary model results, *Geophys. J. Int.*, **115,** 941–959.

Lambeck, K., 1993b. Glacial rebound of the British Isles—II. A high resolution, high-precision model, *Geophys. J. Int.*, **115,** 960–990.

Lambeck, K., Johnston, P., Smither, C. & Nakada, M., 1996. Glacial rebound of the British Isles—III. Constraints on mantle viscosity, *Geophys. J. Int.*, **125,** 340–354.

Longman, I.M., 1962. A Green's function for determining the deformation of the Earth under surface mass loads, 1. Theory, *J. geophys. Res.*, **67,** 845–850.

Longman, I.M., 1963. A Green's function for determining the deformation of the Earth under surface mass loads, 2. Computations and numerical results, *J. geophys. Res.*, **68,** 485–496.

Mao, H.K., Hemley, R.J., Fei, Y., Shu, J.F., Chen, L.C., Jephcoat, A.P., Wu, Y. & Bassett, W.A., 1991. Effect of pressure, temperature and composition on lattice parameters and density of $(Fe, Mg)SiO_3$-perovskites to 30 GPa, *J. geophys. Res.*, **96,** 8069–8079.

McConnell, R.K., Jr, 1965. Isostatic adjustment in a layered earth, *J. geophys. Res.*, **70,** 5171–5188.

Mareschal, J.-C. & Gangi, A.F., 1977. Equilibrium position of a phase boundary under horizontally varying surface loads, *Geophys. J. R. astr. Soc.*, **49,** 757–772.

Mitrovica, J.X., 1996. Haskell [1935] revisited, *J. geophys. Res.*, **101,** 555–569.

Mitrovica, J.X. & Peltier, W.R., 1989. Pleistocene deglaciation and the global gravity field, *J. geophys. Res.*, **94,** 13 651–13 671.

Nakada, M. & Lambeck, K., 1991. Late Pleistocene and Holocene sea-level change; evidence for lateral mantle viscosity structure? in *Glacial Isostasy, Sea-Level and Mantle Rheology,* pp. 33–61, eds Sabadini, R., Lambeck, K. & Boschi, E., Kluwer Academic Publishers, Dordrecht, The Netherlands.

O'Connell, R.J., 1976. The effects of mantle phase changes on post-glacial rebound, *J. geophys. Res.*, **81,** 971–974.

O'Connell, R.J. & Wasserburg, G.J., 1967. Dynamics of the motion of

a phase change boundary to changes in pressure, *Rev. Geophys.*, **5**, 329–410.
Peltier, W.R., 1974. The impulse response of a Maxwell earth, *Rev. Geophys. Space Phys.*, **12**, 649–669.
Peltier, W.R., 1976. Glacial-isostatic adjustment—II. The inverse problem, *Geophys. J. R. astr. Soc.*, **46**, 669–705.
Peltier, W.R., 1985a. The LAGEOS constraint on deep mantle viscosity: results from a new normal mode method for the inversion of viscoelastic relaxation spectra, *J. geophys. Res.*, **90**, 9411–9421.
Peltier, W.R., 1985b. Mantle convection and viscoelasticity, *Ann. Rev. Fluid Mech.*, **17**, 561–608.
Peltier, W.R. & Andrews, J.T., 1976. Glacial isostatic adjustment—I. The forward problem, *Geophys. J. R. astr. Soc.*, **46**, 605–646.
Peltier, W.R. & Jiang, X., 1996. Mantle viscosity from the simultaneous inversion of multiple data sets pertaining to postglacial rebound, *Geophys. Res. Lett.*, **23**, 503–506.
Peltier, W.R., Drummond, R.A. & Tushingham, A.M., 1986. Post-glacial rebound and transient lower mantle rheology, *Geophys. J. R. astr. Soc.*, **87**, 79–116.
Petersen, N., Vinnik, L., Kosarev, G., Kind, R., Oreshin, S. & Stammler, K., 1993. Sharpness of the mantle discontinuities, *Geophys. Res. Lett.*, **20**, 859–862.
Ringwood, A.E., 1975. *Composition and Petrology of the Earth's Mantle*, McGraw-Hill, New York, NY.
Ringwood, A.E., 1991. Phase transformations and their bearing on the constitution and dynamics of the mantle, *Geochim. Cosmochim. Acta*, **55**, 2083–2110.
Rümpker, G. & Wolf, D., 1996. Viscoelastic relaxation of a burgers half-space—implications for the interpretation of the Fennoscandian uplift, *Geophys. J. Int.*, **124**, 541–555.
Sabadini, R., Yuen, D.A. & Boschi, E., 1982. Polar wandering and the forced responses of a rotating, multilayered, viscoelastic planet, *J. geophys. Res.*, **87**, 2885–2903.
Sammis, C.G., Smith, J.C., Schubert, G. & Yuen, D.A., 1977. Viscosity-depth profile of the Earth's mantle: effects of polymorphic phase transitions, *J. geophys. Res.*, **82**, 3747–3761.
Spada, G., Yuen, D.A., Sabadini, R., Morin, P.J. & Gasperini, P., 1990. A computer-aided, algebraic approach to the post-glacial rebound problem, *Mathematica Journal*, **1**, 65–68.
Turcotte, D.L. & Schubert, G., 1971. Structure of the olivine-spinel phase boundary in the descending lithosphere, *J. geophys. Res.*, **74**, 1458–1474.
Tushingham, A.M. & Peltier, W.R., 1992. Validation of the ICE-3G Model of Würm–Wisconsin Deglaciation using a global data base of relative sea level histories, *J. geophys. Res.*, **97**, 3285–3304.
Wolf, D., 1984. The relaxation of spherical and flat Maxwell earth models and effects due to the presence of the lithosphere, *J. Geophys.*, **56**, 24–33.
Wolf, D., 1985. The normal modes of a layered, incompressible Maxwell half-space, *J. Geophys.*, **57**, 106–117.
Wolf, D., 1991a. Boussinesq's problem of viscoelasticity, *Terra Nova*, **3**, 401–407.
Wolf, D., 1991b. Viscoelastodynamics of a stratified, compressible planet: incremental field equations and short- and long-time asymptotes, *Geophys. J. Int.*, **104**, 401–417.
Wolf, D., 1993. The changing role of the lithosphere in models of glacial isostasy: a historical review, *Global planet. Change*, **8**, 95–106.
Wolf, D., 1994. Lamé's problem of gravitational viscoelasticity: the isochemical, incompressible planet, *Geophys. J. Int.*, **116**, 321–348.
Wu, P., 1978. The response of a Maxwell earth to applied surface mass loads: glacial isostatic adjustment, *MSc thesis*, University of Toronto, Canada.
Wu, P., 1990. Deformation of internal boundaries in a viscoelastic earth and topographic coupling between the mantle and core, *Geophys. J. Int.*, **101**, 213–231.
Wu, P., 1992. Deformation of an incompressible viscoelastic flat earth with power-law creep: a finite element approach, *Geophys. J. Int.*, **108**, 35–51.
Wu, P. & Ni, Z., 1996. Some analytical solutions for the visco-elastic gravitational relaxation of a two-layer non-self gravitating incompressible spherical earth, *Geophys. J. Int.*, **126**, 413–436.
Wu, P. & Peltier, W.R., 1982. Viscous gravitational relaxation, *Geophys. J. R. astr. Soc.*, **70**, 435–485.
Wu, P. & Peltier, W.R., 1983. Glacial isostatic adjustment and the free air gravity anomaly as a constraint on deep mantle viscosity, *Geophys. J. R. astr. Soc.*, **74**, 377–449.
Yuen, D.A., Sabadini, R.C.A., Gasperini, P. & Boschi, E., 1986. On transient rheology and glacial isostasy, *J. geophys. Res.*, **91**, 11 420–11 438.

APPENDIX A: APPLICATION OF THE DIVERGENCE THEOREM FOR LANGRANGIAN VARIABLES

The divergence theorem states that

$$\int_S \mathbf{F}\cdot\mathbf{da} = \int_\tau \nabla\cdot\mathbf{F}\, d\tau, \tag{A1}$$

where $\mathbf{F}$ is a vector field in Eulerian coordinates ($\boldsymbol{r}$), τ is the volume of integration and S is its surface, with $\mathbf{da}$ a vector with magnitude equal to the infinitesimal surface area da and with the direction of the outward-pointing normal to the surface. To obtain a condition for the F_1 component, the divergence theorem is applied to a thin pillbox with faces normal to the $\hat{\boldsymbol{r}}_1$ direction (e.g. Cathles 1975). Then,

$$F_1(r_1+\delta r_1, r_2, r_3) - F_1(r_1, r_2, r_3) = \int_{r_1}^{r_1+\delta r_1} \nabla\cdot\mathbf{F}(r_1', r_2, r_3)\, dr_1',$$
$$\approx \delta r_1 \nabla\cdot\mathbf{F}(r_1, r_2, r_3). \tag{A2}$$

To apply the divergence theorem to a vector field given in Lagrangian coordinates, define a vector field $\mathbf{f}$ in Lagrangian coordinates such that $\mathbf{f}(\mathbf{X}(\mathbf{r})) = \mathbf{F}(\mathbf{r})$, where $\mathbf{X}$ is the initial position of the particle now at position $\mathbf{r}$. The derivative $\partial X_i/\partial\tau_j$ is required to express $\nabla\cdot\mathbf{F}$ in terms of $\mathbf{f}$. With the definition of displacement, $r_i = X_i + u_i$, it follows that

$$r_{i,j} = \delta_{ij} + u_{i,j}, \tag{A3}$$

where differentiation with respect to X_j is implied. The only component involving first-order displacement gradients is

$$r_{1,1} = 1 + u_{1,1} = \begin{cases} 1 + \dfrac{\rho^+ - \rho^-}{\rho^+}, & \text{loading} \\ 1 + \dfrac{\rho^- - \rho^+}{\rho^-}, & \text{unloading} \end{cases}. \tag{A4}$$

Since $r_{1,1} = 1/X_{1,1}$, where $r_{1,1} = \partial r_1/\partial X_1$ and $X_{1,1} = \partial X_1/\partial r_1$, we obtain correct to first order

$$X_{1,1} = \frac{1}{1+u_{1,1}} = 1 - u_{1,1} = \begin{cases} \dfrac{\rho^-}{\rho^+}, & \text{loading} \\ \dfrac{\rho^+}{\rho^-}, & \text{unloading} \end{cases}. \tag{A5}$$

For i and j not both 1, $X_{i,j} = \delta_{ij}$. Now the divergence of the field $\mathbf{F}$ in Eulerian coordinates may be written in terms of the same field $\mathbf{f}$ in Lagrangian coordinates in the phase change region:

$$\nabla\cdot\mathbf{F}(\mathbf{r}) = F_{i,i} = f_{i,j}X_{j,i} = f_{1,1}X_{1,1} + f_{2,2} + f_{3,3}. \tag{A6}$$

If we suppress the dependence on the second and third

coordinates, the divergence theorem (A2) takes the form

$$\begin{aligned} f_1(X_1+\delta X_1)-f_1(X_1) &= F_1(X_1+\delta X_1+u_1(X_1+\delta X_1))-F_1(X_1+u_1(X_1)) \\ &\approx [\delta X_1+u_1(X_1+\delta X_1)-u_1(X_1)](f_{1,1}X_{1,1}+f_{2,2}+f_{3,3}). \end{aligned} \tag{A7}$$

If we assume further that f is of first order, and put for the loading case, $X_1 = r_0$ and $\delta X_1 = h$, we obtain

$$\begin{aligned} f_1^+ - f_1^- &= [h+u(r_0+h)-u(r_0)][f_{i,i}+(X_{1,1}-1)f_{1,1}], \\ &= (\varepsilon-u^-)f_{i,i}, \end{aligned} \tag{A8}$$

where we have used the fact that $\varepsilon = h + u(r_0+h)$ (eq. 1) and have dropped the third-order product $(\varepsilon-u^-)u_{1,1}f_{1,1}$. In the unloading case, $X_1 = r_0 + h$ and $\delta X_1 = -h$, which gives the boundary condition

$$\begin{aligned} f_1^+ - f_1^- &= [-h+u(r_0)-u(r_0+h)][f_{i,i}+(X_{1,1}-1)f_{1,1}] \\ &= (u^+-\varepsilon)f_{i,i}, \end{aligned} \tag{A9}$$

correct to second order.